8-6-2019

An Analytical Approach to Ascertain Saturation-excess Versus Infiltration-excess Overland Flow in Urban and Reference Landscapes

Ryan D. Stewart

Aditi S. Bhaskar

Anthony J. Parolari

Dustin L. Herrmann

Jinshi Jian

See next page for additional authors

Authors

Ryan D. Stewart, Aditi S. Bhaskar, Anthony J. Parolari, Dustin L. Herrmann, Jinshi Jian, Laura A. Schifman, and William D. Shuster

Hydrological Processes, Vol. 33, No. 26 (August 06, 2019): 3349-3363. DOI.

An Analytical Approach to Ascertain Saturation-excess Versus Infiltration-excess Overland Flow in Urban and Reference Landscapes

Ryan D. Stewart
School of Plant and Environmental Sciences, Virginia Polytechnic Institute and State University, Blacksburg, VA
Aditi S. Bhaskar
Department of Civil and Environmental Engineering, Colorado State University, Fort Collins, CO
Anthony J. Parolari
Department of Civil, Construction, and Environmental Engineering, Marquette University, Milwaukee, WI
Dustin L. Herrmann
Oak Ridge Institute for Science and Education Research Participant Program with U.S. Environmental Protection Agency, Cincinnati, OH
Jinshi Jian

School of Plant and Environmental Sciences, Virginia Polytechnic Institute and State University, Blacksburg, VA
Joint Global Change Research Institute, Pacific Northwest National Laboratory, College Park, MD
Laura A. Schifman
Department of Biology, Boston University, Boston, MA
William D. Shuster
United States Environmental Protection Agency, Office of Research and Development, National Risk Management Research Laboratory, Cincinnati, OH

ABSTRACT

Uncontrolled overland flow drives flooding, erosion, and contaminant transport, with the severity of these outcomes often amplified in urban areas. In pervious media such as urban soils, overland flow is initiated via either infiltration-excess (where precipitation rate exceeds infiltration capacity) or saturation-excess (when precipitation volume exceeds soil profile storage) mechanisms. These processes call for different management strategies, making it important for municipalities to discern between them. In this study, we derived a generalized one-dimensional model that distinguishes between infiltration-excess overland flow (IEOF) and saturation-excess overland flow (SEOF) using Green–Ampt infiltration concepts. Next, we applied this model to estimate overland flow generation from pervious areas in 11 U.S. cities. We used rainfall forcing that represented low- and high-intensity events and compared responses among measured urban versus predevelopment reference soil hydraulic properties. The derivation showed that the propensity for IEOF versus SEOF is related to the equivalence between two nondimensional ratios: (a) precipitation rate to depth-weighted hydraulic conductivity and (b) depth of soil profile restrictive layer to soil capillary potential. Across all cities, reference soil profiles were associated with greater IEOF for the high-intensity set of storms, and urbanized soil profiles tended towards production of SEOF during the lower intensity set of storms. Urban soils produced more cumulative overland flow as a fraction of cumulative precipitation than did reference soils, particularly under conditions associated with SEOF. These results will assist cities in identifying the type and extent of interventions needed to manage storm water produced from pervious areas.

1 INTRODUCTION

Overland flow, in which water supplied by precipitation or irrigation ponds on the soil surface and then runs off under the force of gravity, causes erosion, rapid contaminant transport, and flooding. The negative consequences of excess overland flow can be particularly acute in urban areas, where impervious cover minimizes infiltration (Baruch et al., **2018**; Leopold, **1968**). With increases in urbanization, changes in frequency and intensity of precipitation patterns (Niyogi, Lei, Kishtawal, Schmid, & Shepherd, **2017**), and the need to design more socially and ecologically sustainable cities (Tzoulas et al., **2007**), many urban areas are adding green spaces and green infrastructure (Gill, Handley, Ennos, & Pauleit, **2007**; Schifman et al., **2017**). These spaces are intended to reduce the amount of storm water run-off entering already overwhelmed sewer systems, in part by relying on soils to infiltrate some of the overland flow generated from impervious surfaces (Voter & Loheide, **2018**). However, pervious surfaces can also become sources of overland flow, indicating that

such areas represent an important component of overall urban hydrologic response. Understanding the mechanisms and physical factors that determine overland flow generation from pervious surfaces is therefore necessary for quantifying the hydrologic impacts of urbanization.

Surface ponding and overland flow generation occurs via two principal mechanisms: infiltration-excess overland flow, hereafter IEOF, and saturation-excess overland flow, hereafter SEOF (Freeze, **1974**; Horton, **1933**). IEOF is initiated when the rate of water inputs (e.g., direct precipitation, irrigation, or overland flow routed to pervious areas as run-on) exceeds the infiltration rate of the soil. Under one-dimensional vertical flow conditions, infiltration rates typically diminish through time as the hydraulic gradient decreases towards unity, with the infiltration capacity of a soil asymptotically converging to field-saturated soil hydraulic conductivity (Philip, **1969**). The rate at which infiltration capacity decreases is dynamic and interacts with soil capillarity (Stewart & Abou Najm, **2018**) and wetting front depth (Green & Ampt, **1911**; Selker & Assouline, **2017**). By contrast, SEOF is a bottom-up process in the soil profile where moisture fills soil pores in an initially unsaturated volume above a hydraulically restrictive soil layer, bedrock, or the water table (Dunne & Black, **1970**; Loague, Heppner, Ebel, & VanderKwaak, **2010**). If water inputs are sufficient to fill this pore volume, the soil profile becomes saturated and overland flow is initiated. The amount of available pore space is controlled by the initial water content and the depth of the soil profile, and these factors together provide the baseline from which saturated conditions develop.

Because of the different factors that drive IEOF and SEOF, most current analytical models do not include both processes and therefore poorly constrain the conditions and processes that favour IEOF versus SEOF in soil profiles. For example, urban run-off models such as the U.S. Environmental Protection Agency's Storm Water Management Model (EPA-SWMM) emphasize IEOF, whereas rainfall/run-off models developed for forested catchments emphasize SEOF via the variable source area concept (Bartlett, Parolari, McDonnell, & Porporato, **2016**; McDonnell, **2003**). Recent discussions have emphasized that further conceptual refinement is needed (McDonnell, **2013**), particularly to develop an analytical framework that represents SEOF and IEOF as linked processes. To date, however, there has been little progress towards this goal.

The ability to integrate SEOF and IEOF processes together becomes particularly important in urban settings, where heterogeneity in soil conditions and land cover increases the complexity of infiltration and saturation processes (Lim, **2016**; Miles & Band, **2015**). Although infiltration rates of urban soils are commonly analysed as point measurements (Schifman & Shuster, **2018**; Schifman, Tryby, Berner, & Shuster, **2018**; Shuster, Dadio, Drohan, Losco, & Shaffer, **2014**), a lack of understanding exists on which processes drive urban soils to generate run-off. The current paradigm in modelling run-off generation in urban catchments is that IEOF is the dominant overland flow generation process, because storm response in urban streams has been found to be closely related to the connectedness of impervious areas (Shuster, Bonta, Thurston, Warnemuende, & Smith, **2005**). However, pervious areas also affect urban stormflow response, as permeable soils can mitigate the effect of urbanization on peak streamflow (Hopkins et al., **2015**; Smith & Smith, **2015**). Urban development can also modify the soil profile via compaction (Batey, **2009**; Shuster, Dadio, Burkman, Earl, & Hall, **2015**), layering and changes in texture from backfilling, and development of restrictive layers (Herrmann, Schifman, & Shuster, **2018**), all of which can promote shallow or perched water tables and may increase the

likelihood of SEOF. Such overland flow generation mechanisms have not been critically examined in these settings, based either on the current profile characteristics or on shifts that may have occurred in pervious urban areas compared with predevelopment reference profiles. With cities turning towards increasing green or open spaces as part of their water management strategies, understanding propensity of urban soil to produce overland flow can guide the type and extent of storm water run-off management intervention needed.

Rainfall characteristics also affect the type of storm water run-off management intervention required (Figure **1**). At the two extreme ends of the intensity–duration spectrum (i.e., low-intensity, short-duration events associated with the first flush of surface-located pollutants, and high-intensity, long-duration events associated with flood risks), overland flow generation has little relevance for management. Between these extremes, however, rainfall characteristics help determine whether a system will tend towards IEOF or SEOF. High-intensity, short-duration storms are most likely to result in run-off dominated by IEOF, as these events exceed the infiltration capacity of soils. In contrast, low-intensity, long-duration events are not anticipated to overwhelm infiltration capacity but may saturate the available soil storage and result in surface run-off dominated by SEOF. Managing overland flow thus requires addressing multiple run-off pathways that are storm dependent and necessitates understanding such interactions between storm events and soils.

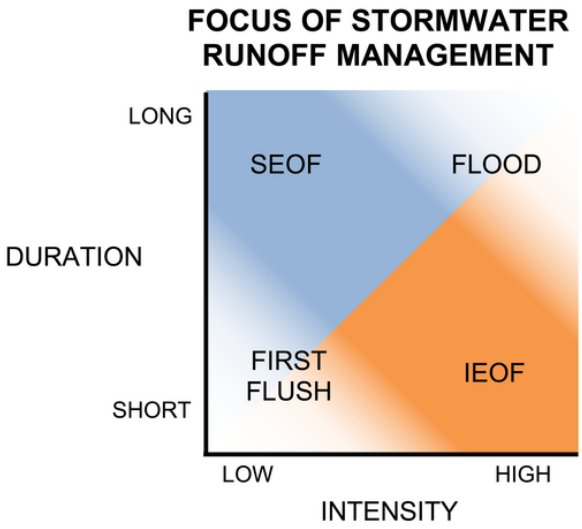

Figure 1 Storm water run-off management may have different emphasis based on the intensity versus duration of precipitation events. Low-intensity, short-duration storms may cause first flush mobilization of deposited pollutants, whereas high-intensity, long-duration storms may cause flood conditions that overwhelm the potential capacity of urban soils to infiltrate and store water. For all other cases, storm water management will depend on whether surface run-off is generated via infiltration-excess overland flow (IEOF) or saturation-excess overland flow (SEOF)

In this study, we test how soil profile characteristics and rainfall forcing affect whether run-off is generated by IEOF or SEOF, and then we assess the influence of urbanization on run-off generation processes. To identify conditions under which IEOF or SEOF dominate run-off generation, the objectives of this study were threefold. For our first objective, we sought to develop an analytic framework that accounts for properties and processes that represent the propensity of a soil profile towards IEOF versus SEOF, based on a one-dimensional vertical treatment that characterizes when and

how these mechanisms activate. Here, we expected that low-permeability soils (i.e., those with low values for saturated hydraulic conductivity) would be more prone to IEOF, whereas soils with shallow restrictive layers would be more prone to SEOF. For our second objective, we aimed to quantify the run-off ratio (overland flow as a fraction of precipitation) based on nondimensional expressions for conditions under which IEOF and SEOF activate. For this objective, we expected that overland flow initiation timing and amounts would vary between the IEOF and SEOF mechanisms. For our third objective, we worked to parameterize the analytical solutions and compare overland flow generation under relatively low- and high-intensity precipitation forcing using an urban and reference (preurban) data set collected in 11 U.S. cities. Here, we anticipated that urban soil profiles would generate more overland flow than would reference soil profiles under both types of precipitation forcing.

2 THEORY

2.1 Evaluating susceptibility to IEOF versus SEOF

To determine whether a soil profile will be more susceptible to IEOF or SEOF, we model a homogenous soil profile with a constant initial water content (ϑ_i [L^3/L^3]) throughout the profile. We assume that the soil has an available soil pore volume, n_e (L^3/L^3), where $n_e = \vartheta_s - \vartheta_i$; that the saturated water content ϑ_s (L^3/L^3) represents the maximum amount of wetting in the unsaturated zone; and that this pore volume sits above an impermeable restrictive layer or water table located at a depth Z (L) from the surface.

We estimate the time to IEOF, t_p (T), using the Green–Ampt infiltration model. The Green–Ampt model assumes that water infiltrates with a sharp wetting front along a hydraulic gradient characterized as $d\Psi/dz = (h_f + z)/z$, where h_f (L) is the wetting front potential, and z (L) is the depth of the wetting front beneath the soil surface and increases downward. The wetting front depth z is related to the cumulative infiltration, I (L), as $z = I/n_e$. Substituting this representation of hydraulic gradient into Darcy's law yields:

$$q = K_s\left(\frac{d\Psi}{dz}\right) = K_s\left(\frac{I + h_f n_e}{I}\right),$$

(1)

where q (L/T) is the infiltration rate and K_s (L/T) is the saturated hydraulic conductivity.

Selker and Assouline (2017) derived the following approximation to Equation 1, which implicitly accounts for cumulative infiltration I when calculating q:

$$q = K_s\left(1 + \frac{A + \sqrt{\frac{n_e h_f}{2K_s t}}}{1 + A\frac{K_s t}{n_e h_f} + \sqrt{\frac{2K_s t}{n_e h_f}}}\right) r > Ks,$$

(2)

where *A* is a constant (typically taken to equal 2/3). As ponding will occur when the infiltration (*q*) and precipitation rates (*r*) are equal, the time to ponding (t_p) is found implicitly using Equation 2 as

$$\frac{r}{K_s} = 1 + \frac{A + \sqrt{\frac{n_e h_f}{2K_s t_p}}}{1 + A\frac{K_s t_p}{n_e h_f} + \sqrt{\frac{2K_s t_p}{n_e h_f}}} \quad r > K_s$$

(3)

We take advantage of the following explicit, approximated expression for time to ponding (discussed further in Appendix A):

$$t_p = \left(\frac{h_f n_e}{r/K_s - 1}\right)\left(\frac{B}{r}\right) \quad r > K_s$$

(4)

where *B* is a constant taken here to equal 5/8.

Next, the saturation-excess ponding condition will occur when the depth of infiltrated precipitation equals the depth of available storage in the profile:

$$I = rt_s = n_e Z,$$

(5)

where t_s (T) represents the time to SEOF. Rearranging Equation 5, we have

$$t_s = n_e Z/r$$

(6)

SEOF will precede IEOF whenever $t_s < t_p$, so combining that inequality with Equations 4 and 6 gives

$$\frac{Z}{h_f} < \left(\frac{B}{\frac{r}{K_s} - 1}\right) r > K_s.$$

(7)

2.2 Simulating overland flow depths under IEOF versus SEOF

As a precursor to quantifying run-off ratio, we first develop expressions for depth of overland flow *OF* (L) at time *t* (T) for both IEOF and SEOF scenarios. We start by assuming that *OF* is equal to the precipitation depth minus the cumulative infiltration, that is, *OF = rt − I.*

In the IEOF case, we normalize Equation 4 as

$$q = K_{\mathrm{s}}\left(1 + \frac{A + \sqrt{\frac{1}{2\tau}}}{1 + A\tau + \sqrt{2\tau}}\right) \quad r > K_{\mathrm{s}},$$

(8)

where τ is a nondimensional form of time (Fok, 1975; Stewart, 2019):

$$\tau = \frac{K_{\mathrm{s}} t}{\mathrm{n_e h_f}},$$

(9a)

$$\tau_{\mathrm{p}} = \frac{K_{\mathrm{s}} t_{\mathrm{p}}}{\mathrm{n_e h_f}}.$$

(9b)

In normalized time, infiltration rate q, and the cumulative infiltration, I, are related:

$$I = \int q dt = \frac{\mathrm{n_e h_f}}{K_{\mathrm{s}}} \int q d\tau.$$

(10)

The nondimensional time to ponding is found implicitly as

$$\frac{r}{K_{\mathrm{s}}} = 1 + \frac{A + \sqrt{1/2\tau_{\mathrm{p}}}}{1 + A\tau_{\mathrm{p}} + \sqrt{2\tau_{\mathrm{p}}}}$$

(11)

noting that Equation 4 can also be used as an explict estimation of time to ponding, with some minor error.

Once the soil ponds, the depth of cumulative infiltration into the matrix will be found by

$$I = \mathrm{n_e h_f}\left(\frac{r}{K_{\mathrm{s}}}\right)\tau_{\mathrm{p}} + \frac{\mathrm{n_e h_f}}{K_{\mathrm{s}}}\int_{\tau_{\mathrm{p}}}^{\tau} q(\tau')\, d\tau' \quad \tau \geq \tau_{\mathrm{p}};\ r > K_{\mathrm{s}},$$

(12)

where τ' is a dummy variable of integration. Integrating Equation 12 using Equation 10 results in

$$I = \mathrm{n_e h_f}\left[\left[\frac{r}{K_\mathrm{s}} - 1\right]\tau_\mathrm{p} + \tau + \ln\left[\frac{1 + A\tau + \sqrt{2\tau}}{1 + A\tau_\mathrm{p} + \sqrt{2\tau_\mathrm{p}}}\right]\right] \quad \tau \geq \tau_\mathrm{p};\ r > K_\mathrm{s}.$$

(13)

Using Equation 13, we can express *OF* as

$$OF = \mathrm{n_e h_f}\left[\left[\frac{r}{K_\mathrm{s}} - 1\right]\left[\tau - \tau_\mathrm{p}\right] - \ln\left[\frac{1 + A\tau + \sqrt{2\tau}}{1 + A\tau_\mathrm{p} + \sqrt{2\tau_\mathrm{p}}}\right]\right] \quad \tau \geq \tau_\mathrm{p};\ r > K_\mathrm{s}.$$

(14)

Equation 14 can also be expressed as a nondimensional quantity using

$$\Gamma = \left(\frac{r}{K_\mathrm{s}} - 1\right)\left(\tau - \tau_\mathrm{p}\right) - \ln\left(\frac{1 + A\tau + \sqrt{2\tau}}{1 + A\tau_\mathrm{p} + \sqrt{2\tau_\mathrm{p}}}\right) \quad \tau \geq \tau_\mathrm{p};\ r > K_\mathrm{s},$$

(15)

where $\Gamma = OF/n_e h_f$.

For SEOF, the nondimensional time to saturation (τ_s) is

$$\tau_\mathrm{s} = \frac{Z/\mathrm{h_f}}{r/K_\mathrm{s}}$$

(16)

Overland flow (*OF*) can be calculated for SEOF as $rt - n_e Z$ or, in nondimensional time, as

$$OF = \mathrm{n_e h_f}\frac{r}{K_\mathrm{s}}(\tau - \tau_\mathrm{s}) \quad \tau \geq \tau_\mathrm{s},$$

(17)

$$\Gamma = \frac{r}{K_\mathrm{s}}(\tau - \tau_\mathrm{s}) \quad \tau \geq \tau_\mathrm{s}.$$

(18)

2.3 Run-off ratio quantification

We next quantify run-off ratio (i.e., *OF*/*R*) for either run-off generation process, using the nondimensional relationship r/K_s that was described in the previous derivation. For IEOF, starting with Equation 14 and $R = rt$, the run-off ratio can be expressed as a function of r/K_s:

$$\frac{OF}{R} = \frac{\tau - \tau_{\mathrm{p}}}{\tau}\left\{1 - \left[1 + \frac{\tau}{\tau - \tau_{\mathrm{p}}}\ln\left[\frac{1 + A\tau + \sqrt{2\tau}}{1 + A\tau_{\mathrm{p}} + \sqrt{2\tau_{\mathrm{p}}}}\right]\right]\left\{\frac{r}{K_s}\right\}^{-1}\right\} \quad \tau \geq \tau_p.$$

(19)

Similarly, using Equation 17 to derive the run-off ratio for SEOF, we have

$$\frac{OF}{R} = 1 - \frac{\tau_s}{\tau} = 1 - \left(\frac{Z}{h_f \tau}\right)\left(\frac{r}{K_s}\right)^{-1} \quad \tau \geq \tau_s.$$

(20)

Both relationships (19) and (20) have the following general form:

$$\frac{OF}{R} = a\left[1 - b\left(\frac{r}{K_s}\right)^{-1}\right]$$

(21)

with the parameters *a* and *b* for IEOF and SEOF given in Table 1. When both *a* and *b* are unity, our derivation indicates a steep rise in run-off ratio as the ratio r/K_s exceeds 1 (i.e., when the precipitation rate starts to exceed the hydraulic conductivity of the near-surface soil).

Table 1. Assignment of values to variables *a* and *b* for infiltration-excess overland flow (IEOF) and saturation-excess overland flow (SEOF) conditions, based on Equations 19–21

Variable	IEOF	SEOF
a	$\tau \geq \tau_p$	1
b	$1 + \frac{\tau}{\tau - \tau_{\mathrm{p}}}\ln\left(\frac{1 + A\tau + \sqrt{2\tau}}{1 + A\tau_{\mathrm{p}} + \sqrt{2\tau_{\mathrm{p}}}}\right)$	$\left(\frac{Z}{h_f \tau}\right)$

3 METHODS

3.1 Field data

Urban soil profiles were assessed in 11 cities across the United States: A = Atlanta, GA (number of soil profiles *n* = 15); C = Camden, NJ (*n* = 28); D = Detroit, MI (*n* = 57); I = Cincinnati, OH (*n* = 67); J = San Juan, PR (*n* = 26); N = New Orleans, LA (*n* = 19); O = Omaha, NE (*n* = 36); P = Portland, ME (*n* = 67); T = Tacoma, WA (*n* = 17); V = Cleveland, OH (*n* = 127); X = Phoenix, AZ (*n* = 13). Infiltration rates were measured at the surface using a tension infiltrometer (Mini-Disk Tension Infiltrometer; METER Group, Pullman, USA) with source pressure head h_s = −2 cm. Measured data were used as a proxy for saturated hydraulic conductivity (K_s) following the method of Zhang (**1997**). Subsurface infiltration rates were measured using a borehole permeameter, and the Glover solution (Zangar, **1953**) was used to infer K_s from those data. For each urban profile, a corresponding reference (i.e., predevelopment) soil profile was developed as in Herrmann et al. (**2018**), which involved expert input from U.S.

Department of Agriculture Natural Resources Conservation Service soil scientists with knowledge specific to each city.

3.2 Model parameterization

In the urban profiles, Z was constrained by the depth of the first soil layer that was field identified as being hydraulically restrictive with the presence of fragipans (i.e., dense layers that restrict water movement and root growth), the presence of redoximorphic features as an indication of seasonal water table development, an abrupt shift to a finer-textured soil horizon, or K_s < 0.1 cm/hr (Thomas, Conta, Severson, & Galbraith, **2016**). If no restrictive layers were observed, Z was set as the bottom of the lowest soil layer assessed. For the reference profiles, Z was also set at the top of any restrictive layer (i.e., K_s < 0.1 cm/hr) or the bottom of lowest reported layer. To estimate other soil hydraulic properties, we used the measured per cent sand, silt, and clay data, along with any reported data (e.g., bulk densities for both urban and reference profiles; and water retention data for reference profiles). These data were input into random forest pedotransfer function (PTF) models that were trained to provide values for the van Genuchten (**1980**) water retention parameters ϑ_r, ϑ_s, α, and m, along with K_s for any soil layer in which that property had not been measured directly via field assessments. More information on the PTF models is provided in Appendix **B**.

Individual-layer K_s values were compiled into a single representative K_s for each profile using the technique described by Oosterbaan and Nijland (1994):

$$K_s = Z / \sum_{j=1}^{n} D_i / K_{s,i},$$

(22)

where D is the thickness of each layer i.

Likewise, individual-layer ϑ_s values were compiled into a single depth-weighted ϑ_s for each profile by

$$\theta_s = \frac{1}{Z} \sum_{i-1}^{n} \theta_{s,i} D_i,$$

(23)

To simulate similar conditions across cities, the available pore space n_e for the profile was assumed to equal $0.75\vartheta_s$. This value represented moderately dry initial conditions that still included some antecedent moisture.

The wetting front potential h_f was estimated using the following equation (Morel-Seytoux et al., 1996):

$$\mathrm{h_f} = \left(\frac{1}{\alpha}\right)\left(\frac{0.046m + 2.07m^2 + 19.5m^3}{1 + 4.7m + 16m^2}\right),$$

(24)

where α and m represent the van Genuchten water retention parameters. We used the surface layer h_f value to represent the entire profile.

Values of Z/h_f and r/K_s were then calculated for each soil profile, with K_s estimated by Equation **22**. Individual soil profiles were then aggregated to provide per-city means and errors for K_s, h_f, Z, and n_e; K_s was calculated as a geometric mean with 95% confidence intervals, whereas h_f, Z, and n_e were calculated as arithmetic means along with standard errors of the means.

Next, simulations for each profile were forced with 2-year recurrence interval storms of 1- and 24-hr durations, with storms calculated for each city (Bonnin et al., **2006**; Miller, Frederick, & Tracey, **1973**). The precipitation durations (i.e., 1 and 24 hr) were normalized as τ using Equation (9) along with estimated K_s, h_f, and n_e values for each soil profile. The mean precipitation rates r (L/T) were calculated as total precipitation R (L) divided by duration t (T). The times to ponding and saturation were also calculated for each combination of soil profile and precipitation intensity using Equations **11** and **16**. Whenever $\tau < \tau_p < \tau_s$, overland flow depths OF and Γ were calculated using Equations **14** and **15**; whenever $\tau < \tau_s < \tau_p$, overland flow depths were calculated using Equations **17** and **18**. Run-off ratios were calculated for each location and event as total overland flow OF over cumulative precipitation R and according to Equations **19** and **20**. The constants a and b were also calculated for each profile that generated overland flow using Equation **21**. To assess the potential influence of urbanization on soil properties and overland flow depths, we compared per-city values of ln (K_s), h_f, Z, n_e, and OF (from the 1- and 24-hr storms) between urban and reference profiles using paired t tests ($\alpha = 0.05$).

4 RESULTS

4.1 Susceptibility to IEOF versus SEOF

Using our model framework, we found that IEOF and SEOF occurrence is differentiated by the behaviour of two nondimensional variables: precipitation rate normalized to hydraulic conductivity, r/K_s, and soil depth normalized to wetting front potential, Z/h_f. Figure **2** shows the theoretical propensity for IEOF compared with SEOF, as estimated by Equation **7**. Conditions where the precipitation rate r far exceeds K_s lead to greater IEOF propensity, whereas SEOF is the only possible run-off generation mechanism if r is less than K_s. If the depth of the soil profile Z is much smaller than wetting front potential h_f, SEOF can occur even when r/K_s is greater than 1. A shallower soil profile (smaller Z) takes less water to saturate completely, whereas a large wetting front potential drives a greater initial infiltration rate, reducing the propensity for IEOF and increasing that for SEOF.

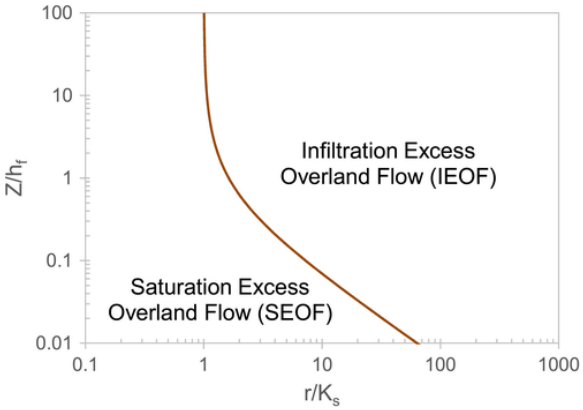

Figure 2 Delineation of conditions that favour IEOF versus SEOF, as quantified by Equation 7 assuming B = 5/8. r/K_s represents the nondimensional ratio of precipitation rate to saturated hydraulic conductivity, and Z/h_f represents the nondimensional ratio of soil profile depth to wetting front potential

After overland flow is initiated by IEOF or SEOF, the model simulates the accumulation of nondimensional overland flow (Γ; Equations **15** and **18**) over time in a way that depends on both the run-off generation mechanism and r/K_s. Our derivation relied on shifting to a nondimensional time frame, which showed that the rate of overland flow increases through time for IEOF (Figure **3**a) while remaining linear for SEOF (Figure **3**b). As values of r/K_s increase, overland flow depth accumulates faster for both IEOF and SEOF, but overland flow depth accumulates in different ways for IEOF and SEOF. For IEOF, when precipitation rate nominally exceeds hydraulic conductivity (r/K_s = 1.2), overland flow accumulates more slowly, and to a smaller cumulative depth, than when r/K_s is larger.

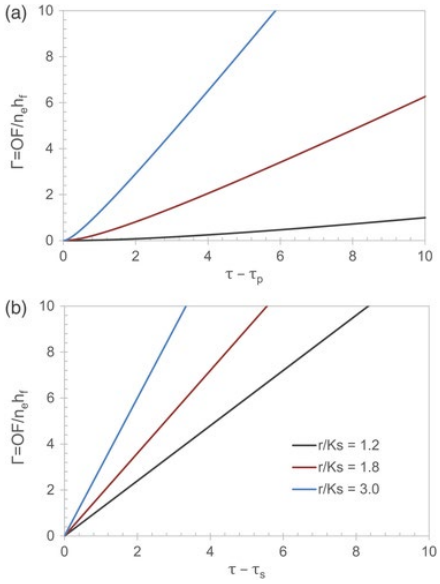

Figure 3 Nondimensional overland flow depth Γ versus nondimensional time, τ, for (a) infiltration-excess overland flow and (b) saturation-excess overland flow, shown here for r/K_s values of 1.2, 1.8, and 3

4.2 Reference and urban soil profile properties

Next, we investigated the soil characteristics in reference and urban soil profiles. For most cities (i.e., Atlanta, Detroit, Cincinnati, Cleveland, Omaha, Portland, and Tacoma), the geometric mean of depth-weighted K_s values was lower for urban than for reference profiles (Figure **4**a), though the differences

were not significant for Atlanta, Cincinnati, or Omaha (paired *t* test; $p \geq .05$). For other cities (i.e., Camden, San Juan, New Orleans, and Phoenix), the mean reference K_s was lower than the urban mean K_s, although the difference was not significant for Camden (paired *t* test; $p \geq .05$). The wetting front potential was generally higher in urban soil profiles compared with reference profiles (Figure **4**b), though San Juan, New Orleans, and Tacoma all had significantly smaller h_f values in the urban profiles (paired *t* tests; $p < .05$). Six of the cities (Atlanta, New Orleans, Omaha, Portland, Tacoma, and Cleveland) had shallower depths to restrictive layers (Z) when urbanized (Figure **4**c). In four of the cities (Atlanta, Camden, Omaha, and Phoenix), Z was constrained for the reference profiles by the limit of collected data and in reality may have extended even deeper than reported, as the urban profile depths for Camden and Omaha both had depths of more than 250 cm. For most cities, the available pore space was lower in urban soil profiles than in reference profiles, though differences were minor: overall mean $n_e = 0.341$ in the reference profiles and $n_e = 0.324$ in the urban profiles (data not shown).

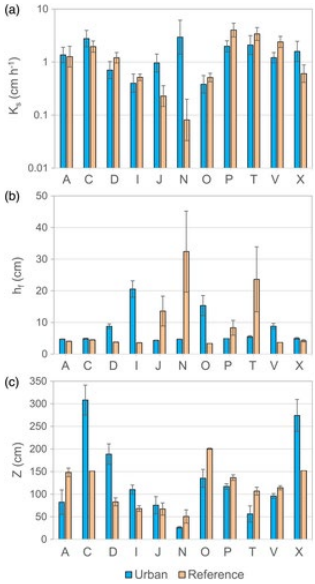

Figure 4 Per-city mean values of (a) K_s, (b) h_f, and (c) Z for reference and urban profiles. K_s values are presented as geometric means ±95% confidence intervals; h_f and Z values are presented as arithmetic means ± standard errors of the means. A = Atlanta, GA; C = Camden, NJ; D = Detroit, MI; I = Cincinnati, OH; J = San Juan, PR; N = New Orleans, LA; O = Omaha, NE; P = Portland, ME; T = Tacoma, WA; V = Cleveland, OH; X = Phoenix, AZ. Asterisks (*) indicate significant differences between urban and reference values (paired *t* test; $p < .05$)

4.3 Urbanization effects on susceptibility to IEOF versus SEOF

The nondimensional hydraulic characteristics Z/h_f (depth-normalized wetting front potential) and r/K_s (relative precipitation rate) were compiled for the 11 cities. Here, city-specific precipitation rates were quantified for 1- and 24-hr durations based on a 2-year return period (Figure **5**). For all soils and both precipitation durations, the propensity towards IEOF or SEOF (as modelled by Equation **7**) was more strongly controlled by the relative precipitation rate (r/K_s) than the depth-normalized wetting front potential (Z/h_f). With the 1-hr duration, nearly all reference and urban soils were estimated to experience IEOF before SEOF (Figure **5**a). The exceptions were Tacoma, which even under the higher 1-hr precipitation intensity exhibited a tendency towards SEOF in both urban and reference conditions, and the reference profiles in Portland. For the 24-hr duration, SEOF was estimated to be the most likely run-off generation mechanism (Figure **5**b). Here, the two exceptions were the reference

profiles from San Juan and New Orleans, which, due to relatively low K_s values (Figure **4**a), were still more likely to produce surface run-off via IEOF.

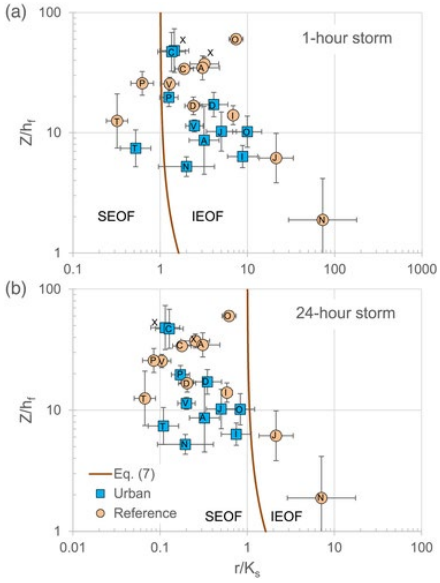

Figure 5 Nondimensional hydraulic characteristics (Z/h_f versus r/K_s) of 11 U.S. cities for (a) 1- and (b) 24-hr storms with 2-year recurrence intervals. Note shift in *x*-axis scaling. Points indicate geometric mean values; error bars indicate 95% confidence intervals. Equation 7 was applied assuming B = 5/8. A = Atlanta, GA; C = Camden, NJ; D = Detroit, MI; I = Cincinnati, OH; J = San Juan, PR; N = New Orleans, LA; O = Omaha, NE; P = Portland, ME; T = Tacoma, WA; V = Cleveland, OH; X = Phoenix, AZ. IEOF, infiltration-excess overland flow; SEOF, saturation-excess overland flow

At the level of individual soil profiles, changes imposed by urbanization also altered both the type and magnitude of run-off generation for different storm intensities and durations (Figure **6**). For the 1-hr, 2-year set of storms, urbanization caused a mixed response in terms of the total proportion of profiles that produced overland flow via combined IEOF and SEOF. In Atlanta, Camden, Tacoma, and Cleveland, more profiles produced overland flow after urbanization compared with the reference profiles, whereas Cincinnati, New Orleans, Omaha, Portland, and Phoenix had the opposite response (Figure **6**a,b). Detroit and San Juan had no change for this particular set of storm events. Most profiles, whether urban or reference, produced surface run-off via IEOF, with only a small number of urban profiles in Atlanta and New Orleans producing SEOF. For the lower intensity 24-hr, 2-year set of storms, urbanization not only increased the number of profiles that generated overland flow but also increased the proportion of profiles that generated run-off by the SEOF mechanism (Figure **6**c,d). Atlanta, Camden, San Juan, New Orleans, and Cleveland all had the majority of overland flow produced via SEOF during this set of lower intensity storms, due to shallow soil profiles (represented by small values of Z) found in those cities.

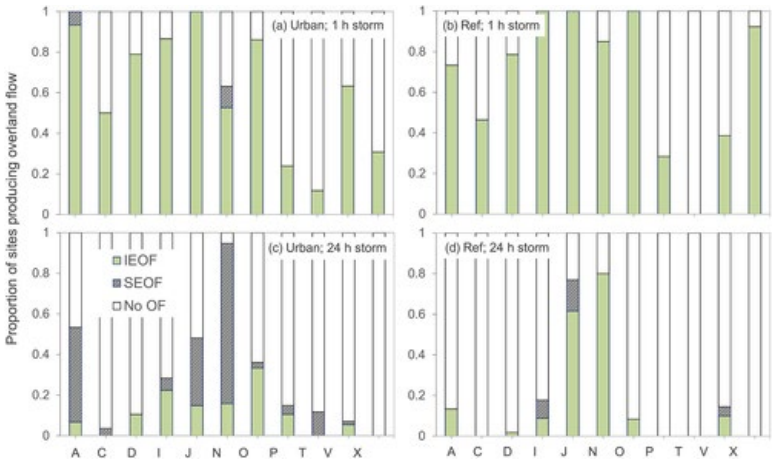

Figure 6 Proportion of profiles in each city that produce overland flow, and whether that generation was through infiltration-excess overland flow (IEOF) or saturation-excess overland flow (SEOF). Profiles that did not produce overland flow are labelled "No OF." (a, b) One-hour, 2-year storms; (c, d) 24-hour, 2-year storms. (a, c) Postdevelopment profiles ("Urban"); (b, d) predevelopment reference profiles ("Ref"). A = Atlanta, GA; C = Camden, NJ; D = Detroit, MI; I = Cincinnati, OH; J = San Juan, PR; N = New Orleans, LA; O = Omaha, NE; P = Portland, ME; T = Tacoma, WA; V = Cleveland, OH; X = Phoenix, AZ

4.4 Urbanization effects on cumulative overland flow

The effects of urbanization on cumulative overland flow depended on precipitation intensity. Cumulative overland flow for the 1-hr, 2-year storms was either similar or higher in the reference soil profiles as compared with the urban soil profiles (Figure **7**a). Specifically, Phoenix, Cincinnati, Camden, Omaha, San Juan, and New Orleans all had higher estimated overland flow amounts in the predevelopment reference state. Although this finding can be explained by the higher K_s values estimated for the urban soils in Phoenix, Camden, San Juan, and New Orleans (Figure **4**a), the differences for Cincinnati and Omaha corresponded to larger h_f values in urban compared with reference profiles (Figure **4**b).

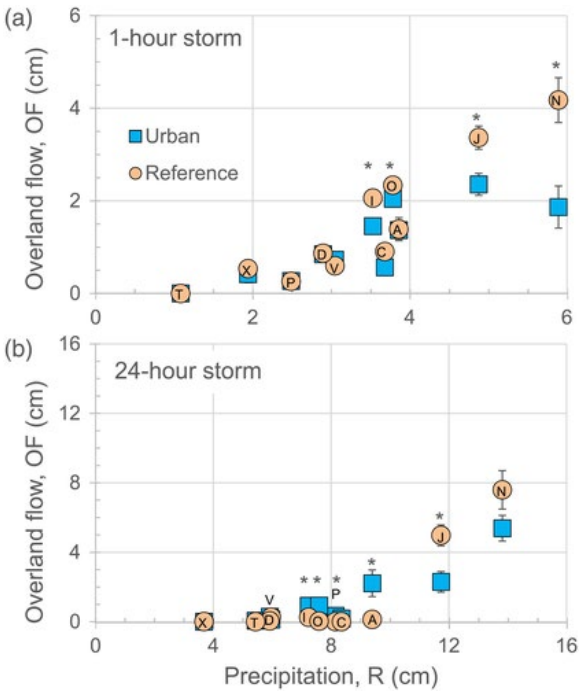

Figure 7 Estimations of cumulative overland flow, *OF* (cm), based on cumulative precipitation, *R* (cm), for (a) 1- and (b) 24-hr storms with 2-year recurrence intervals. Urban represents measured values after urbanization; reference indicates predevelopment characteristics. Points indicate mean values; error bars indicate standard errors of the mean. A = Atlanta, GA; C = Camden, NJ; D = Detroit, MI; I = Cincinnati, OH; J = San Juan, PR; N = New Orleans, LA; O = Omaha, NE; P = Portland, ME; T = Tacoma, WA; V = Cleveland, OH; X = Phoenix, AZ. Asterisks (*) indicate significant differences between urban and reference values (paired *t* test; $p < .05$)

By contrast, the reference soil profiles had equal or lower amounts of overland flow for the 24-hr, 2-year storms, with the exceptions of San Juan and New Orleans, where the reference profiles still had greater overland flow depths compared with the urban ones (Figure **7**b). Those two cities (San Juan and New Orleans) both had relatively high 24-hr, 2-year precipitation amounts and relatively low reference K_s values (Figure **4**a). For the remaining profiles, urbanization was associated with smaller depth-normalized wetting front potential (i.e., smaller Z/h_f values; Figure **5**) and therefore less time to saturation (Equation **16**).

4.5 Urbanization effects on run-off ratio

The run-off ratio response (i.e., cumulative overland flow as a fraction of cumulative precipitation, OF/R) was modeled for both sets of precipitation events using Equation **21** and mean values for a and b. These curves showed a threshold near $r/K_s = 1$, beyond which run-off ratio rapidly increased as the relative rainfall rate increased (Figure **8**). The use of actual field data for different soils detailed variability in how run-off ratio responds, especially with regard to the spread of data across the range of r/K_s. Under the set of 1-hr storms, most of the overland flow was attributed to infiltration excess, and the urban and reference profiles had similar responses (Figure **8**a). Under the lower intensity 24-hr storms, however, the run-off ratio varied substantially between reference and urban soil profiles (Figure **8**b). Many urban soils produced more cumulative overland flow as a fraction of cumulative precipitation than did reference soils. The differences were most pronounced for $r/K_s \leq 1$, which represents conditions associated with SEOF. For both sets of storms, certain soil profiles

generated lower *OF*/*R* than estimated by Equation **21**, primarily under IEOF conditions (i.e., $r/K_s > 1$). These soil profiles were characterized by high h_f values, which meant that they could infiltrate more water before ponding.

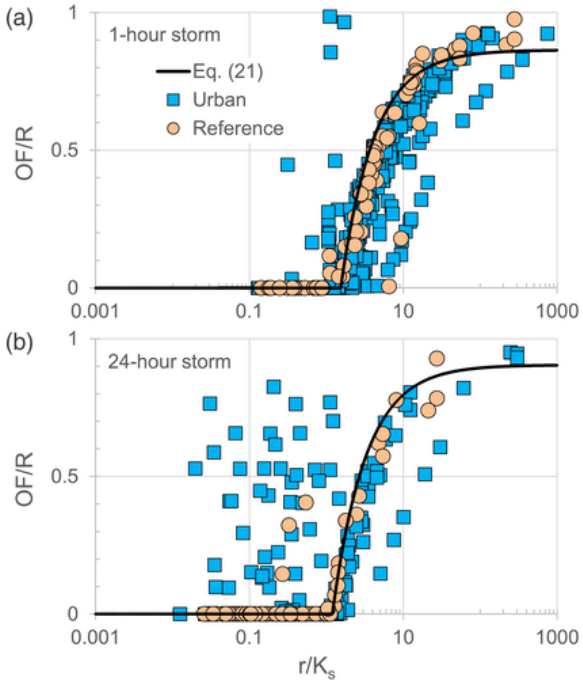

Figure 8 Run-off ratio (*OF*/*R*) as a function of r/K_s, with *r* estimated using (a) a 1-hr, 2-year storm and (b) a 24-hr, 2-year storm. Urban represents measured values after urbanization; reference indicates predevelopment characteristics. Equation 21 was plotted using mean values for *a* and *b* based on all samples (*a* = 0.864 and *b* = 1.54for the 1-hr storm; *a* = 0.905 and *b* = 1.20 for the 24-hr storm)

5 DISCUSSION

An analytical model was developed to evaluate the propensity of soil profiles to produce surface run-off via IEOF versus SEOF. Three factors were important to this analysis: depth-averaged saturated hydraulic conductivity, K_s; wetting front potential, h_f; and depth to restrictive layer, *Z.* Small values of the first two parameters favoured run-off generation via IEOF, whereas small values for *Z* favoured SEOF (Figure **2**).

The model was used to analyse how run-off initiation timing and amounts vary between overland flow processes. The results showed that, for a given precipitation rate, SEOF will accumulate overland flow more rapidly than for any IEOF scenario, because during IEOF some water will continue to infiltrate, whereas all precipitation become overland flow during SEOF (Figure **3**). Still, even though SEOF produces more overland flow than does IEOF after ponding or saturation occurs, the time to these conditions are not equivalent. For $r/K_s > 1$, unless *Z* is quite small or h_f is quite large, IEOF will begin earlier than SEOF (Figure **2**). Thus, infiltration excess can produce more overland flow than can surface excess, depending on specific storm and soil characteristics.

Next, the model was used to interpret how changes in soil profiles and hydraulic properties imposed by urbanization impact run-off generation mechanisms and overland flow depths (Figure **4**). In the data set described here, urbanization increased the propensity of SEOF during long-duration, low-intensity

storms. However, in some cases, urbanization ameliorated IEOF that can occur during high-intensity storm events. By casting the critical model parameters (K_s, h_f, and Z) and precipitation rate (r) into two nondimensional numbers, r/K_s and Z/h_f, our analysis was able to place soil profiles for 11 cities as being initially susceptible to either SEOF or IEOF under two different storm intensities (Figures **5** and **6**). The model was then used to estimate overland flow as cumulative amounts (Figure **7**) and as proportion of precipitation (Figure **8**).

The results revealed a nuanced picture of the hydrologic changes that urbanization can induce. For instance, four of the cities were estimated to have increased K_s values in urban versus reference profiles, reflecting better ability to absorb precipitation. Likewise, seven of the cities had higher h_f values in the urban profiles, again indicating better infiltration capacity. However, the urban profiles had smaller Z values, signifying less storage in the profile before saturation. As a result of these shifts between urban and reference profile properties, many of the cities had less estimated overland flow during high-intensity events (represented by 1-hr, 2-year storms) under urban compared with reference conditions. Under low-intensity events, however, urban profiles tended to generate more overland flow than did reference ones, due to saturation effects. As a result, urbanization appears to increase the range of conditions under which many soils will produce overland flow, even if the total accumulated depths may be reduced in certain locations (e.g., in New Orleans, LA, and San Juan, PR, which had relatively high urban K_s values; Figure **4**) and under certain conditions (e.g., high-intensity rains in Cincinnati, OH).

Our analysis focused only on identifying the initial overland flow generation mechanism that is likely to act on a soil profile. As a consequence, we assumed that a soil profile will respond to precipitation forcing by either SEOF or IEOF, but not both. Previous work has suggested that certain soils may experience both run-off generation mechanisms over the course of changing precipitation (Yang, Li, Sun, & Ni, **2015**). Our model could therefore underestimate run-off generation in soils that were characterized as having IEOF run-off generation (i.e., $\tau_p < \tau_s$) if those soils were to saturate during the course of an event. Because the urban soils analysed here were more likely to have small Z/h_f values, it is possible that overland flow was underestimated in some profiles, particularly for the 24-hr, 2-year events.

Here, we note that our analysis obscured the role of available pore space, n_e, in overland flow processes. For one, in our analysis, we assumed that the nondimensional quantity developed to delineate IEOF and SEOF (i.e., Equation **7**) is independent of available pore space n_e. Although this result is valid for a uniform vertical distribution of available pore space (e.g., the uniformly distribution of $n_e = 0.75\vartheta_s$ we assumed), it will not hold true whenever available pore space varies with depth. As soil profiles often have increasing water content with depth, the solution posed here trades some realism in exchange for simplicity required from an analytical model. Our assumption of $n_e = 0.75\vartheta_s$ meant that the soils were treated as being fairly dry at the beginning of the event. This assumption likely minimized the potential effect of that term in actual overland flow generation, as both SEOF and IEOF will occur more rapidly in initially wet soils. We also assumed that the initial wetting front potential h_f can be treated as a constant with minimal effect on results, although in reality h_f will decrease as the initial water content increases (see Stewart, Rupp, Najm, & Selker, **2013**, or Stewart & Abou Najm, **2018**, for more discussion of this point). Even so, under our assumption of

75% available pore space volume ($\vartheta_i > \sim 0.75\vartheta_s$), the wetting front potential can be approximated as a constant nearly equal to the maximum value found in completely dry soil.

We chose to use depth-averaged K_s values in our analysis (Equation **22**) to better integrate changes throughout the soil profile that occurred during urbanization. This approach is valid for one-dimensional flow under conditions where the hydraulic gradient through each layer can adjust to maintain steady-state (and typically saturated) flow through different soil layers (Bos, **1994**). If the surface/near-surface layer is the most hydraulically restrictive, however, this assumption may not be valid, as excess water can be removed via overland flow before the gradient adjusts. This discrepancy could result in underestimates for overland flow in cases where the lowest K_s values occur at or near the surface. In the data set tested here, 99 out of 472 urban profiles and 83 out of 472 reference profiles had surface K_s values that were less than half as large as the profile-weighted K_s values. However, only four of the urban profiles (and no reference profiles) had surface K_s values more than one order of magnitude smaller than the profile average. The uncertainty associated with this assumption should thus be small in this case, though additional scrutiny may be required in other applications.

The model also considered soils as simplified one-dimensional profiles, thus ignoring factors such as surface topography and landscape connectivity. In urban systems, run-on from impervious surfaces can contribute additional water to pervious surfaces. This additional flow may result in quicker saturation, which may impact the processes and timing at which point overland flow starts in comparison with reference landscapes (Voter & Loheide, **2018**). Surface topography also can play an important role in run-off generation, both by altering the amount of infiltration that occurs in sloping versus flat surfaces (Chen & Young, **2006**) and by increasing wetness in low-lying and convergent portions of the landscape (Zimmer & McGlynn, **2018**). Still, the parameters identified here as being most important to run-off generation likely act as primary controls on overland flow in more complex settings.

Despite the aforementioned assumptions and simplifications, the model confers the ability to characterize most likely run-off generation mechanisms and captures differential responses induced by precipitation intensity versus duration (Dunkerley, **2016**; Dunkerley, **2018**; Masselink et al., **2016**). The model was developed using an original and comprehensive data set collected in 11 cities across the U.S. The cities studied here varied widely in climate type (Kottek, Grieser, Beck, Rudolf, & Rubel, **2006**), and the soil profiles included all 12 textures recognized by the U.S. Department of Agriculture National Resources Conservation Service (Soil Survey Staff, **2014**) and possessed a range of soil properties (e.g., Z, h_f, and K_s). These results are therefore likely to be representative of conditions found in many other urban areas around the world. At the same time, the model framework developed here should be applicable to any agency or municipality charged with urban water management.

In terms of specific intervention strategies, cities with urban soil profiles prone to IEOF could be best suited for interventions that increase infiltration capacity, thus maximizing the precipitation rate at which overland flow is initiated. Some strategies to augment infiltration rates include using refined demolition practices (U.S. Environmental Protection Agency, **2013**) or subsoiling (Schwartz & Smith, **2016**), maintaining vegetation over the long term to protect the soil surface and preserve organic matter content, and increasing surface roughness, so as to concomitantly promote infiltration and mitigate against overland flow formation. For SEOF, targeted management strategies could be to

reduce the additional water inputs that could lead to saturation (impervious surfaces draining to pervious surfaces or urban landscape irrigation) while increasing available pore space in the soil profile or breaking up subsurface restrictive layers.

Our findings show that, for long-duration storms, SEOF is more common in urban soils than in their predevelopment reference counterparts, emphasizing the need to increase soil capacity for storing storm water. At the same time, SEOF may be even more prevalent in urban soils than estimated here due to additional water that becomes delivered from adjacent impervious areas during storm events. Future climate projections also indicate a shift in precipitation regimes to less frequent storm events but greater precipitation loads per event. If this shift results in a greater occurrence of low-intensity, long-duration storms, a focus on SEOF management will become increasingly appropriate for urban areas.

6 SUMMARY AND CONCLUSIONS

In this study, we used Green–Ampt infiltration concepts in a nondimensional framework to identify propensity towards IEOF versus SEOF. Overland flow generation type varied as a function of rainfall rate over depth-weighted hydraulic conductivity (r/K_s) versus depth of the soil profile restrictive layer to soil capillary potential (Z/h_f). Field measurements collected in 11 U.S. cities showed that, compared with the predevelopment reference condition, urbanization often increased K_s and h_f, leading many of the cities to produce less surface run-off via IEOF. However, urbanization also led to shallower restrictive layer depths (Z), meaning that many cities may be more prone to SEOF during low-intensity, long-duration storms.

The model output presented here highlights run-off generation processes from direct catch inputs of precipitation. We developed and applied this model to urban areas, due to our ability to compare and contrast soil profiles and the open questions regarding the effects of urbanization on precipitation partitioning in pervious areas. Still, these concepts can apply to other systems in which overland flow is generated by both IEOF and SEOF. Some examples could be other nonforested landscapes where IEOF is important, such as those with little vegetative cover (e.g., burned watersheds, fallow agricultural areas, and arid watersheds). Even though the approach does make a number of simplifications, such as assuming uniform and homogenous one-dimensional vertical profiles, it still allows assessment of the relative likelihood of two important run-off generation processes based on a few parameters that can be easily measured in the field.

This work could be complemented by field monitoring of conditions that lead to overland flow from urban pervious areas and the correspondence of these field conditions to important parameters in the analytical model developed. A greater understanding of the conditions under which pervious urban areas can infiltrate water and the limiting factors to infiltration (whether this is soil depth or saturated hydraulic conductivity) could help inform urban water managers. An example application could be mapping areas such as lawns that can infiltrate additional water from disconnected downspouts versus those that may generate overland flow and contribute to flooding during storm events. Finally, the results presented here highlight that urbanization can induce distinct hydrological responses across cities, thus emphasizing the importance of having straightforward analytical tools, such as the one presented here, when designing interventions.

DATA AVAILABILITY STATEMENT

Data from this paper are permanently archived at **https://data.lib.vt.edu/files/00000011h**.

LIST OF VARIABLES

ϑ_i initial water content (L^3/L^3)

ϑ_s saturated water content (L^3/L^3)

ϑ_r residual water content (L^3/L^3)

α van Genuchten (1980) water retention model parameter (L^{-1})

m van Genuchten (1980) water retention model parameter (−)

n_e available soil pore volume (L^3/L^3)

Z depth to impermeable soil layer or water table (L)

$d\Psi/dz$ hydraulic gradient (L/L)

h_f wetting front potential (L)

z depth of wetting front beneath soil surface (L)

I cumulative infiltration (L)

q infiltration rate (L/T)

K_s saturated hydraulic conductivity (L/T)

r precipitation rate (L/T)

R cumulative precipitation (L)

t time since beginning of precipitation event (T)

t_p time to ponding due to infiltration excess (T)

t_s time to ponding due to saturation excess (T)

τ nondimensional time, $\tau = K_s t/n_e h_f$ (−)

OF cumulative overland flow (L)

Γ nondimensional overland flow, $\Gamma = OF/n_e h_f$ (−)

A constant in infiltration model, assumed to equal 2/3

B constant in infiltration model, assumed to equal 5/8

a parameter for run-off ratio (OF/R) model (−)

b parameter for run-off ratio (OF/R) model (−)

n number of soil profiles

$\boldsymbol{D_i}$ thickness of soil layer *i* (L)

ACKNOWLEDGMENTS

Funding for this work was provided in part by the Virginia Agricultural Experiment Station and the Hatch Program of the National Institute of Food and Agriculture, U.S. Department of Agriculture. The research was performed while D.L. Herrmann held a postdoctoral research participant appointment administered by the Oak Ridge Institute for Science and Education through Interagency Agreement DW-8992433001 between the U.S. Department of Energy and the U.S. Environmental Protection Agency (EPA) at the National Risk Management Research Laboratory within the Office of Research and Development of the U.S. EPA. The views expressed in this paper are those of the authors and do not necessarily represent the views or policies of the U.S. EPA.

APPENDIX A: ALTERNATIVE APPROXIMATION FOR TIME TO PONDING

The Green–Ampt model states that

$$q = K_s\left(\frac{d\Psi}{dz}\right) = K_s\left(\frac{I + h_{\mathrm{f}} n_e}{I}\right),$$

(A1)

where q (L/T) is the infiltration rate, K_s (L/T) is the saturated hydraulic conductivity, $d\Psi/dz$ is the hydraulic gradient (L/L), h_{f} (L) is the wetting front potential, n_e is the available pore space, and I is the cumulative infiltration (L).

Ponding will occur when the infiltration rate matches the precipitation rate, r (L/T); therefore, substituting $q = r$ into Equation A1 and rearranging gives

$$I_{\mathrm{p}} = \frac{\mathrm{h_f n_e}}{r/K_s - 1} \quad r > K_s,$$

(A2)

where I_{p} (L) is the depth of infiltration at the time of ponding. Because $t_{\mathrm{p}} = I_p/r$, Equation A2 can be solved as

$$\tau_{\mathrm{p}} = \left(\frac{1}{r/K_s - 1}\right)\left(\frac{K_s}{r}\right) \quad r > K_s,$$

(A3)

where $\tau_{\mathrm{p}} = K_s t_{\mathrm{p}}/n_e h_{\mathrm{f}}$.

In the Selker and Assouline (2017) approximation, the normalized time to ponding (τ_{p}) is found implicitly by

$$\frac{r}{K_s} = 1 + \frac{A + \sqrt{\frac{1}{2\tau_\mathrm{p}}}}{1 + A\tau_\mathrm{p} + \sqrt{2\tau_\mathrm{p}}} \quad r > K_s.$$

(A4)

The time to ponding τ_p values given by Equation A3 versus A4 are not equivalent; however, by modifying Equation A3 with a parameter *B*, we can obtain a "universal" approximation for time to ponding with the Green–Ampt family of models:

$$\tau_\mathrm{p} = \left(\frac{1}{r/K_s - 1}\right)\left(B\frac{K_s}{r}\right) \quad r > K_s.$$

(A5)

When $B = 1$, Equation A5 becomes equal to Equation A3, whereas when $B \approx 5/8$, the time to ponding τ_p values estimated by Equations A4 and A5 become nearly identical (Figure A1). Therefore, we can use Equation A5 with $B = 5/8$ to obtain a close explicit approximation for time of ponding when working with the Selker and Assouline (2017) expression.

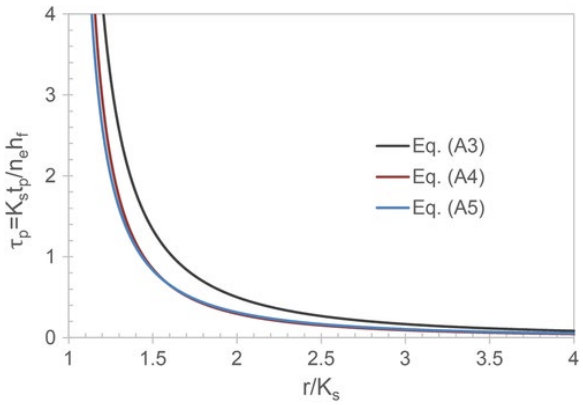

Figure A1 Estimated normalized time to ponding as a function of relative precipitation rate for three models. Equation A4 was plotted with $A = 2/3$, and Equation A5 was plotted with $B = 5/8$

APPENDIX B: DEVELOPMENT OF PEDOTRANSFER FUNCTIONS

We estimated missing values for K_s and the van Genuchten (**1980**) water retention parameters ϑ_r, ϑ_s, α, and m by developing PTFs using random forest modelling. The K_s model was trained using 711 observations collected in 12 cities (i.e., the 11 cities included in this study plus nine urban profiles assessed in Majuro, Republic of the Marshall Islands). Of those 711 observations, 228 were from the reference profiles (each representing a unique record), using the K_s values reported in the National Cooperative Soil Survey database. The other 543 K_s values were measured in the urban profiles using either surface-placed tension infiltrometers or subsurface borehole tests. The model inputs were categorical soil texture or per cent sand, silt, and clay, the latter selected when available (Figure **B1**). In total, the PTF models were used to estimate K_s for 1,790 urban soil layers and 21 reference soil layers

that did not have measured values, whereas measured K_s values for retained for 2,690 records (1,876 reference and 814 urban soil layers).

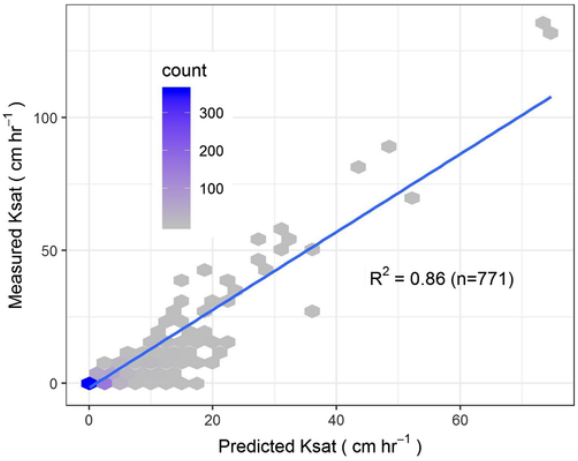

Figure B1 K_s predicted using the random forest pedotransfer function developed in this study versus measured K_s values. Input data for the pedotransfer function model are per cent sand, silt, and clay; the blue line indicates linear regression results

To estimate water retention parameters, data were compiled from 1,871 samples in the National Cooperative Soil Survey (**2019**) database. The first step required estimating van Genuchten (**1980**) model parameters (ϑ_r, ϑ_s, α, and m) for each sample based on measured water contents at 0, −60, −100, −330, and − 15,000 cm. The optimal water retention parameters for each sample were fit using a Markov chain Monte Carlo approach. We then used random forest modelling to analyse the relationship between water retention parameters, soil textural components (i.e., per cent sand, silt, and clay), categorical soil texture, bulk density, and soil water contents at −330 and − 15,000 cm. Due to input data disparities, we ultimately developed four different random forest models for each van Genuchten parameter, each using one of the following sets of inputs: (a) categorical soil texture; (b) per cent sand, silt, and clay (Figure **B2**); (c) per cent sand, silt, and clay and bulk density; and (d) per cent sand, silt, and clay, bulk density, and water contents at −330 and − 15,000 cm. The reference profiles had 127 layers analysed using the first PTF model (soil texture) and 1,773 layers that were analysed using the fourth PTF model (per cent sand, silt, and clay, bulk density, and water contents at −330 and − 15,000 cm). The urban profiles had 1,830 records that were analysed using the first PTF model, 701 record analysed using the second PTF (per cent sand, silt, and clay), and 70 records analysed using the third PTF (per cent sand, silt, and clay plus bulk density).

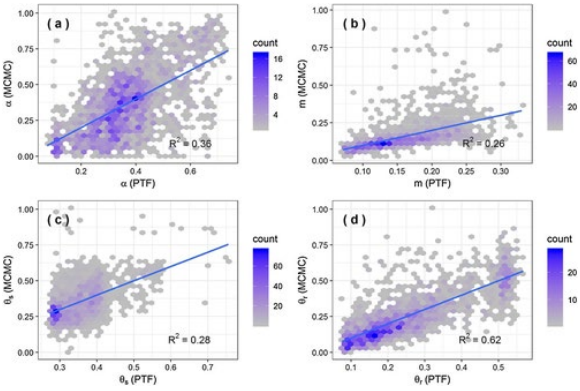

Figure B2 Predicted parameters using a random forest model for the van Genuchten (1980) water retention parameters—(a) α, (b) m, (c) ϑ_r, and (d) ϑ_s—versus parameter values that were constrained from measured data using a Markov chain Monte Carlo (MCMC) approach. Input data for the pedotransfer function (PTF) model are per cent sand, silt, and clay; the blue lines indicate linear regression results

References

Bartlett, M. S., Parolari, A. J., McDonnell, J. J., & Porporato, A. (2016). Framework for event-based semidistributed modeling that unifies the SCS-CN method, VIC, PDM, and TOPMODEL. *Water Resources Research*, **52**, 7036– 7056. https://doi.org/10.1002/2016wr019084

Baruch, E. M., Voss, K. A., Blaszczak, J. R., Delesantro, J., Urban, D. L., & Bernhardt, E. S. (2018). Not all pavements lead to streams: Variation in impervious surface connectivity affects urban stream ecosystems. *Freshwater Science*, **37**, 673– 684. https://doi.org/10.1086/699014

Batey, T. (2009). Soil compaction and soil management—A review. *Soil Use and Management*, **25**, 335– 345. https://doi.org/10.1111/j.1475-2743.2009.00236.x

Bonnin, G. M., Martin, D., Lin, B., Parzybok, T., Yekta, M., & Riley, D. (2006). Precipitation-frequency atlas of the United States. *NOAA atlas*, **14**, 1– 65.

Bos, M. (1994). Basics of groundwater flow. In H. P. Ritzema (Ed.), *Drainage principles and applications* (pp. 225– 261). Wageningen, The Netherlands: International Institute for Land Reclamation and Improvement.

Chen, L., & Young, M. H. (2006). Green–Ampt infiltration model for sloping surfaces. *Water Resources Research*, **42**. https://doi.org/10.1029/2005wr004468

Dunkerley, D. (2016). An approach to analysing plot scale infiltration and runoff responses to rainfall of fluctuating intensity. *Hydrological Processes*, **31**, 191– 206. https://doi.org/10.1002/hyp.10990

Dunkerley, D. (2018). How is overland flow produced under intermittent rain? An analysis using plot-scale rainfall simulation on dryland soils. *Journal of Hydrology*, **556**, 119– 130. https://doi.org/10.1016/j.jhydrol.2017.11.003

Dunne, T., & Black, R. D. (1970). Partial area contributions to storm runoff in a small New England watershed. *Water Resources Research*, **6**, 1296– 1311. https://doi.org/10.1029/WR006i005p01296

Fok, Y.-S. (1975). A comparison of the Green–Ampt and Philip two-term infiltration equations. *Transactions of ASAE*, **18**, 1073– 1075.

Freeze, R. A. (1974). Streamflow generation. *Reviews of Geophysics*, **12**, 627– 647. https://doi.org/10.1029/RG012i004p00627

Gill, S. E., Handley, J. F., Ennos, A. R., & Pauleit, S. (2007). Adapting cities for climate change: The role of the green infrastructure. *Built Environment*, **33**, 115– 133. https://doi.org/10.2148/benv.33.1.115

Green, W. H., & Ampt, G. (1911). Studies on soil physics. *Journal of Agricultural Science*, **4**, 1– 24. https://doi.org/10.1017/S0021859600001441

Herrmann, D. L., Schifman, L. A., & Shuster, W. D. (2018). Widespread loss of intermediate soil horizons in urban landscapes. *Proceedings of the National Academy of Sciences*, **115**, 6751– 6755. https://doi.org/10.1073/pnas.1800305115

Hopkins, K. G., Morse, N. B., Bain, D. J., Bettez, N. D., Grimm, N. B., Morse, J. L., … Suchy, A. K. (2015). Assessment of regional variation in streamflow responses to urbanization and the persistence of physiography. *Environmental Science & Technology*, **49**, 2724– 2732. https://doi.org/10.1021/es505389y

Horton, R. E. (1933). The role of infiltration in the hydrologic cycle. *Eos, Transactions American Geophysical Union*, **14**, 446– 460. https://doi.org/10.1029/TR014i001p00446

Kottek, M., Grieser, J., Beck, C., Rudolf, B., & Rubel, F. (2006). World map of the Köppen–Geiger climate classification updated. *Meteorologische Zeitschrift*, **15**, 259– 263. https://doi.org/10.1127/0941-2948/2006/0130

Leopold, L. B. (1968). *Hydrology for urban land planning: A guidebook on the hydrologic effects of urban land use* (Vol. **554**) (pp. 1– 18). Washington, DC: US Department of the Interior, Geological Survey.

Lim, T. C. (2016). Predictors of urban variable source area: A cross-sectional analysis of urbanized catchments in the United States. *Hydrological Processes*, **30**, 4799– 4814. https://doi.org/10.1002/hyp.10943

Loague, K., Heppner, C. S., Ebel, B. A., & VanderKwaak, J. E. (2010). The quixotic search for a comprehensive understanding of hydrologic response at the surface: Horton, Dunne, Dunton, and the role of concept-development simulation. *Hydrological Processes*, **24**, 2499– 2505.

Masselink, R. J. H., Heckmann, T., Temme, A. J. A. M., Anders, N. S., Gooren, H. P. A., & Keesstra, S. D. (2016). A network theory approach for a better understanding of overland flow connectivity. *Hydrological Processes*, **31**, 207– 220. https://doi.org/10.1002/hyp.10993

McDonnell, J. J. (2003). Where does water go when it rains? Moving beyond the variable source area concept of rainfall-runoff response. *Hydrological Processes*, **17**, 1869– 1875. https://doi.org/10.1002/hyp.5132

McDonnell, J. J. (2013). Are all runoff processes the same? *Hydrological Processes*, **27**, 4103– 4111. https://doi.org/10.1002/hyp.10076

Miles, B., & Band, L. E. (2015). Green infrastructure stormwater management at the watershed scale: Urban variable source area and watershed capacitance. *Hydrological Processes*, **29**, 2268– 2274. https://doi.org/10.1002/hyp.10448

Miller, J. F., Frederick, R. H., & Tracey, R. J. (1973). Precipitation-frequency atlas of the western United States.

Morel-Seytoux, H. J., Meyer, P. D., Nachabe, M., Touma, J., van Genuchten, M. T., & Lenhard, R. J. (1996). Parameter equivalence for the Brooks-Corey and van Genuchten soil characteristics: Preserving the effective capillary drive. *Water Resources Research*, **32**, 1251– 1258. https://doi.org/10.1029/96WR00069

National Cooperative Soil Survey. (2019). National Cooperative Soil Survey characterization database. United States Department of Agriculture Natural Resources Conservation Service.

Niyogi, D., Lei, M., Kishtawal, C., Schmid, P., & Shepherd, M. (2017). Urbanization impacts on the summer heavy rainfall climatology over the eastern United States. *Earth Interactions*, **21**, 1– 17.

Oosterbaan, R., & Nijland, H. (1994). Determining the saturated hydraulic conductivity. In H. P. Ritzema (Ed.), *Drainage principles and applications* (pp. 435– 476). Wageningen, The Netherlands: International Institute for Land Reclamation and Improvement.

Philip, J. R. (1969). Theory of infiltration. In V. T. Chow (Ed.), *Advances in hydroscience* pp. 215– 296). Cambridge, MA: Academic Press.

Schifman, L. A., Herrmann, D. L., Shuster, W. D., Ossola, A., Garmestani, A., & Hopton, M. E. (2017). Situating green infrastructure in context: A framework for adaptive socio-hydrology in cities. *Water Resources Research*, **53**, 10139– 10154. https://doi.org/10.1002/2017wr020926

Schifman, L. A., & Shuster, W. D. (2018). Comparison of measured and simulated urban soil hydrologic properties. *Journal of Hydrologic Engineering*, **24**, 04018056.

Schifman, L. A., Tryby, M. E., Berner, J., & Shuster, W. D. (2018). Managing uncertainty in runoff estimation with the US Environmental Protection Agency National Stormwater Calculator. *JAWRA Journal of the American Water Resources Association*, **54**, 148– 159. https://doi.org/10.1111/1752-1688.12599

Schwartz, S. S., & Smith, B. (2016). Restoring hydrologic function in urban landscapes with suburban subsoiling. *Journal of Hydrology*, **543**, 770– 781. https://doi.org/10.1016/j.jhydrol.2016.10.051

Selker, J., & Assouline, S. (2017). An explicit, parsimonious, and accurate estimate for ponded infiltration into soils using the Green and Ampt approach. *Water Resources Research*, **53**, 7481– 7487. https://doi.org/10.1002/2017wr021020

Shuster, W. D., Bonta, J., Thurston, H., Warnemuende, E., & Smith, D. (2005). Impacts of impervious surface on watershed hydrology: A review. *Urban Water Journal*, **2**, 263– 275. https://doi.org/10.1080/15730620500386529

Shuster, W. D., Dadio, S., Drohan, P., Losco, R., & Shaffer, J. (2014). Residential demolition and its impact on vacant lot hydrology: Implications for the management of stormwater and sewer system overflows. *Landscape and Urban Planning*, **125**, 48– 56. https://doi.org/10.1016/j.landurbplan.2014.02.003

Shuster, W. D., Dadio, S. D., Burkman, C. E., Earl, S. R., & Hall, S. J. (2015). Hydropedological assessments of parcel-level infiltration in an arid urban ecosystem. *Soil Science Society of America Journal*, **79**, 398– 406. https://doi.org/10.2136/sssaj2014.05.0200

Smith, B. K., & Smith, J. A. (2015). The flashiest watersheds in the contiguous United States. *Journal of Hydrometeorology*, **16**, 2365– 2381. https://doi.org/10.1175/JHM-D-14-0217.1

Soil Survey Staff (2014). *Keys to soil taxonomy* (12th ed.). Washington, DC: USDA-NRCS. US Gov. Print. Office.

Stewart, R. D. (2019). A generalized analytical solution for preferential infiltration and wetting. *Vadose Zone Journal*, **18**, 18. https://doi.org/10.2136/vzj2018.08.0148

Stewart, R. D., & Abou Najm, M. R. (2018). A comprehensive model for single ring infiltration. 1: Influence of initial water content and soil hydraulic properties. *Soil Science Society of America Journal*, **82**, 548– 557. https://doi.org/10.2136/sssaj2017.09.0314

Stewart, R. D., Rupp, D. E., Najm, M. R. A., & Selker, J. S. (2013). Modeling effect of initial soil moisture on sorptivity and infiltration. *Water Resources Research*, **49**, 7037– 7047. https://doi.org/10.1002/wrcr.20508

Thomas, S. K., Conta, J. F., & Severson, E. D., Galbraith, J. M. (2016). Measuring saturated hydraulic conductivity in soil. Virginia Cooperative Extension, pp: 1– 13.

Tzoulas, K., Korpela, K., Venn, S., Yli-Pelkonen, V., Kaźmierczak, A., Niemela, J., & James, P. (2007). Promoting ecosystem and human health in urban areas using green infrastructure: A literature review. *Landscape and Urban Planning*, **81**, 167– 178. https://doi.org/10.1016/j.landurbplan.2007.02.001

U.S. Environmental Protection Agency. (2013). On the road to reuse: Residential demolition bid specification development tool.

van Genuchten, M. T. (1980). A closed-form equation for predicting the hydraulic conductivity of unsaturated soils. *Soil Science Society of America Journal*, **44**, 892– 898. https://doi.org/10.2136/sssaj1980.03615995004400050002x

Voter, C., & Loheide, S. (2018). Urban residential surface and subsurface hydrology: Synergistic effects of low-impact features at the parcel scale. *Water Resources Research*, **54**, 8216– 8233. https://doi.org/10.1029/2018WR022534

Yang, W.-Y., Li, D., Sun, T., & Ni, G.-H. (2015). Saturation-excess and infiltration-excess runoff on green roofs. *Ecological Engineering*, **74**, 327– 336. https://doi.org/10.1016/j.ecoleng.2014.10.023

Zangar, C. N. (1953). Theory and problems of water percolation. U.S. Bureau of Reclamation.

Zhang, R. (1997). Infiltration models for the disk infiltrometer. *Soil Science Society of America Journal*, **61**, 1597– 1603. https://doi.org/10.2136/sssaj1997.03615995006100060008x

Zimmer, M. A., & McGlynn, B. L. (2018). Lateral, vertical, and longitudinal source area connectivity drive runoff and carbon export across watershed scales. *Water Resources Research*, **54**, 1576– 1598. https://doi.org/10.1002/2017wr021718